scientific reports

Check for updates

OPEN

Nitrogen-doped carbon-based phenolic resin loaded with Pd NPs for hydrodechlorination of 4-Chlorophenol

Zhengyu Pan[1,2,3], Xianlang Chen[1,2,3], Zijian Wang[2], Rongrong Li[2], Tongyang Song[1,2], Yuhao Cai[2], Deman Han[2]✉ & Jianrong Chen[1]✉

The catalytic hydrodechlorination (HDC) technology exhibits great flexibility and safety under mild conditions, and shows extremely promising application prospects for the degradation of 4-Chlorophenol (4-CP). Prepare the N-doped phenolic resin carbon support (PMF) using phenol, melamine and formaldehyde as raw materials, and load Pd nanoparticles (NPs) on it. The XPS results indicate that the Pd/PMF-800 has a higher Pyridine-N (24.8%) and a higher $Pd^0/(Pd^{2+}+Pd^0)$ ratio (65.4%). Moreover, the difference in electronegativity between the N atom and the resin carbon support enhances the binding energy between them. This enhancement promotes the nucleation of Pd NPs on the surface of the resin carbon support, thereby imparting higher stability to the Pd NPs. Due to these comprehensive advantages, Pd/PMF-800 has the highest dechlorination activity (k_{obs} = 0.0594 min^{-1}) and stability (dechlorination rate is 91.56% after 5 cycle). Additionally, it also demonstrates efficient dehalogenation rates for 2-Chlorophenol and 4-Bromophenol. It can provide a catalyst that has high-efficiency dehalogenation performance, strong acid and alkali stability and adaptability, and can be recycled for the degradation of halogenated phenols in the environment.

Keywords Hydrodechlorination (HDC), 4-Chlorophenol (4-CP), Resin modification, Synergistic effect, Pd nanoparticles (NPs)

Chlorophenols (CPs) are widely used in various industrial processes, including the production of herbicides, insecticides, dyes, disinfectants, plant regulators, and wood preservatives[1–3]. During the production process, wastewater containing varying concentrations of CPs is generated, which enters the environment through various pathways. Due to its acute toxicity and poor biodegradability, it poses a serious threat to the ecological environment and human health[4–6]. Traditional water treatment technologies, such as activated carbon, microporous carbon fibers, or carbon nanotubes have been employed for adsorption and removal of CPs[2,7]. However, when its adsorption capacity is exhausted, only a small amount of adsorbent can be reused, and most adsorbents are prone to secondary pollution. Among various detoxification technologies, including adsorption[8–10], biodegradation[11–13], photocatalysis[14–16], electrochemical oxidation[17–20], and Hydrodechlorination (HDC)[2,3,21–24], researchers have found that HDC technology has emerged as an environmentally friendly and effective method to decompose stable C-Cl bonds and convert toxic CPs into safer and more valuable compounds[25,26]. This detoxification technology for removing CPs has the advantages of high flexibility, low energy consumption, and process safety[27]. Pd/AC, Pd /CNTs, Pd/Fh (mesoporous ferrihydrite), Pd-Ni/γAl_2O_3-SiO_2 catalysts have been confirmed by research to be effective in HDC[7,28–30], the activity and stability of different Pd-based catalysts for the hydrodechlorination of 4-CP are shown in Table 1. However, the practical application of Pd-based catalysts is limited by issues such as high cost, decreased activity or even deactivation in multiple catalytic cycles. Therefore, it is necessary to further develop catalysts with high performance and low cost.

Polymer resin carbon catalysts have been widely applied in the chemical and pharmaceutical industries. Polymer resins have high surface area, enhanced porosity, adjustable pore size distribution, and surface functional groups, which can remove specific pollutants[31]. These characteristics enable resins carbon to be used as catalyst carrier materials, especially when selectivity, stability, and ease of recovery are important considerations. In

[1]College of Geography and Environmental Sciences, Zhejiang Normal University, Jinhua 321004, China. [2]Engineering Research Center of Recycling & Comprehensive Utilization of Pharmaceutical and Chemical Waste of Zhejiang Province, Taizhou University, Taizhou 318000, Zhejiang, China. [3]Zhengyu Pan and Xianlang Chen contributed equally to this work. ✉email: hdm@tzc.edu.cn; cjr@zjnu.cn

Catalyst	Activity (%)	Stability(%)(after three cycles)
Pd/AC	92.2	–
Pd/Fh	100	82
Pd/CNTs	6<	–

Table 1. Activity and stability of different Pd-based catalysts for the hydrodechlorination of 4-CP.

recent years, Zhou et al. developed Co-based resin carbon catalysts that activate persulfate to produce SO^{4-} and·OH for the degradation of ibuprofen, achieving a degradation rate of over 70%[32]. Zhao et al. developed a Cu-based resin carbon catalyst for methanol oxidative carbonylation to produce dimethyl carbonate, achieving a 5% conversion rate for methanol and 100% selectivity for dimethyl carbonate[33]. In a study by Macarena et al., Pd-supported spherical activated carbon based on polymer was developed and applied in the HDC of 4-CP in the aqueous phase under similar environmental conditions. The catalyst demonstrated high dechlorination ability during 100 h of continuous experiments[34]. However, during the use of these catalysts, changes in pH value can lead to a decrease in their catalytic activity, and it becomes difficult to control the size of the nanoparticles. Therefore, it is crucial to develop new Pd-based resin carbon catalysts to improve catalytic performance.

Doping heteroatoms in carbon materials has been widely used as an effective method to regulate the electronic and chemical properties of carbon materials[35–38]. The heteroatoms commonly used for doping carbon materials include B, N, P, S etc. Due to the different sizes and electronegativity of different heteroatoms, the properties of carbon materials doped with different heteroatoms vary. N-doped is the most widely used and has expanded to multiple fields such as supercapacitors[39–41], fuel cells[42–44], photocatalytic sensors[45], biosensors[46–49]. Melamine is widely used as an N precursor for doping carbon materials due to its low price, easy availability, and suitability for large-scale applications. Ze et al. prepared nitrogen doped carbon materials for absorbing carbon dioxide using a melamine nitrogen source. The porosity of the carbon material reached 97.6%, the surface area was 1406 m^2/g, and the heteroatom nitrogen content was 0.98–2.09%[50]. Li et al. used melamine as a nitrogen source and successfully prepared four non-metallic carbon nitride catalysts with different nitrogen contents by changing the amount of melamine, which were used in the acetylene hydrochlorination reaction[51]. Hu et al. prepared N-doped agarose derived porous carbon electrode materials with high specific capacitance and long cycle life using melamine as a nitrogen source through a one-step activation doping method[52]. N-doped can enhance the electrical conductivity, specific surface area, and pore structure of carbon materials. Additionally, N-doped can also alter the catalytic activity of carbon materials.

In this work, three phenolic resin carbons with different N contents were prepared using melamine as the N source and by varying the carbonization temperature. The synergistic effect of adjusting N-doped and N content was utilized to optimize the phenolic resin carbon support. After loading Pd NPs, Pd/PMF exhibits excellent catalytic performance in the HDC reaction of 4-CP in aqueous phase. We characterize and analyze the appearance, elemental composition, degree of graphitization, chemical structure, and loading amount of the catalyst through TEM, ICP, XRD, Raman, XPS and FTIR. The effects of pH and temperature on the reaction of 4-CP HDC were investigated and catalytic hydrogenation dehalogenation of 2-Chlorophenol (2-CP) and 4-Bromophenol (4-BP). Finally, investigate the stability of catalysts in multiple 4-CP removal cycles. All results indicate that the prepared Pd/PMF-800 can serve as a promising catalyst for the 4-CP HDC reaction.

Materials and methods

Chemicals

Phenol (C_6H_6OH, 99%), 4-Chlorophenol (C_6H_5ClO, 99%), melamine ($C_3H_6N_6$, 99%), sodium hydroxide (NaOH, 98%), 2-Chlorophenol (C_6H_5ClO, 99%) and 4-Bromophenol (C_6H_5BrO, 98%) were purchased from Shanghai McLean Biochemical Technology Co., Ltd. Formaldehyde (CH_2O, 37%, 13.16 mol/L-14.23 mol/L) was purchased from Zhejiang Sanying Chemical Reagent Co., Ltd. Cyclohexanone ($C_6H_{10}O$, 99.5%, 9.65 mol/L) and cyclohexanol ($C_6H_{12}O$, 98%, 9.66 mol/L) were from Shanghai Runjie Chemical Reagent Co., Ltd. Hydrochloric acid (HCl, 36%, 11 mol/L-11.64 mol/L) was purchased from Zhejiang Hanno Chemical Technology Co., Ltd. $PdCl_2$ (99%) was purchased from Sa'en Chemical Technology (Shanghai) Co., Ltd. High-purity hydrogen gas (H_2, 99%) used as the hydrogen source was purchased from Taizhou Gas Co., Ltd. Activated carbon (AC) was purchased from Shanghai Chemical Reagent Factory, China. All chemical substances used in the experiments are of analytical grade, and deionized water was employed for all procedures. All chemicals were used as received without further purification.

Catalyst Preparation

Co-condensed resin (PMF) was synthesized via a sol-gel process followed by freeze-drying, as reported by Li et al.[50]. Firstly, phenol, melamine, and formaldehyde were dissolved in a single-neck flask at a molar ratio of 1:1:2.5. The pH was adjusted to 8 using a 10 mol/L sodium hydroxide solution. The mixture was then heated in a water bath at 90 °C for 1 h to obtain the PMF, which was subsequently sealed in a glass container and cured at 100 °C for 24 h. The resulting solid PMF was carbonized in a tubular furnace at temperatures of 700 °C, 800 °C, and 900 °C for 4 h as control samples, with all other conditions held constant. The prepared PMF samples were denoted as PMF-700, PMF-800, and PMF-900, respectively.

The Pd-based catalyst was synthesized using a wet impregnation method. A specific amount of PMF was dispersed in deionized water, and a $PdCl_2$ solution (5 mg/mL) was added. The mixture was stirred for 4 h, filtered, and then vacuum-dried at 80 °C. Subsequently, the catalyst was subjected to a temperature of 300 °C for

2 h in a hydrogen atmosphere to obtain 1% Pd-loaded Pd/PMF. As a control, 1% Pd/AC was prepared under the same conditions. Weigh 500 mg of $PdCl_2$ and place it in a beaker. Add 1 mL of hydrochloric acid and 9 mL of deionized water, then sonicate the mixture. After $PdCl_2$ is completely dissolved, transfer the solution into a 100 mL volumetric flask and add deionized water to make up the volume to 100 mL.

Catalytic HDC experiment

A series of experiments were conducted for the HDC of 4-CP in a magnetic high-pressure parallel reactor (WP-MSAR-500 A, Xi'an Huatai Kesi Chemical Technology Co., Ltd). To prepare the contaminated solution, 1200 mg of 4-CP was added to 100 mL of pure water to obtain a 4-CP concentration of 12 mg/mL. Subsequently, 1 mL of the resulting solution was transferred to a 10 mL quartz glass reaction tube, and then 10 mg of each synthesized catalyst was added to the reaction tube. High-purity hydrogen gas was introduced into the reaction vessel, and it was purged three times to ensure complete removal of air from the reaction vessel. The hydrogen gas pressure in the reaction vessel was maintained at 0.1 MPa. When the temperature of the reaction vessel reached the preset temperature, stirring was initiated. After every 10 min of reaction, 10 µL of the reaction mixture was sampled at room temperature using a micropipette, a total of 8 times. The samples were extracted with ethyl acetate and stored in a vial for further analysis. This study utilized a Shimadzu gas chromatograph equipped with a 5MS/Sil column (0.25 mm×30 mm×0.25 µm) to determine the concentration of 4-CP in the samples. The analysis was performed with the 5MS/Sil column at 260 ℃.

Characterization

The morphology and distribution of Pd NPs were determined by TEM. Determine the crystal structure in composite materials through XRD. Analyze the degree of graphitization of the carrier through Raman. Analyze the effect of different carbonization temperatures on the chemical structure of the carrier using FTIR. Analyze the valence state, element types and nitrogen types of Pd NPs in the catalyst using XPS. Determine the loading amount of Pd in the catalyst using ICP-OES.

Mass transfer limitation

Evaluate the mass transfer rate inside and outside the particles, judging the impact of mass transfer on catalytic activity. Based on the slip velocity method proposed by Hariott[53], calculate the total liquid-solid mass transfer rate coefficient (k_c), and evaluate the liquid-solid mass transfer rate outside the particles. The transmission rate of a single ball is given by a semi theoretical equation[53]:

$$N_{sh} = \frac{k_c D_c}{D_v} = 2 + 0.6\left(\frac{D_c v \rho}{\mu_d}\right)^{0.5}\left(\frac{\mu_d}{\rho D_v}\right)^{0.33} \quad (1)$$

where N_{Sh} is Sherwood number, D_c is diameter of catalyst, D_v is diffusion coefficient of 4-CP in water, v is the average velocity of the fluid, ρ is solution density, μ_d indicates dynamic viscosity of the solution. The infinite dilution diffusion coefficient of the non-electrolyte in water was estimated using the Hayduk-Loudie formula[54]:

$$D_v = \frac{13.26 \times 10^{-5}}{\mu_s^{1.4} V_Z^{0.589}} \quad (2)$$

where μ_s is viscosity of the solvent, V_Z is volume of solute molecular at normal boiling point. The mass transfer rate constant was then calculated by multiplying the k_c by the geometric surface area of the catalyst per volume of the solution[31], a:

$$a = \frac{S_c x m}{\rho_c x V_c} x \frac{1}{V} \quad (3)$$

where S_c is geometric surface area of the catalyst, V_c is geometric volume of the catalyst, m is the mass of the catalyst in the reactor tube, ρ_c is the catalyst particle density, V is the reactor tube volume. Using the Weisz and Prater standards[55] evaluate the liquid-solid mass transfer limitations within particles, which are the ratio of reaction and diffusion rate, was used:

$$\frac{k_{obs} D_c^2}{D_e} \quad (4)$$

Obtaining reaction rate constant k_{obs} through fitting, D_c is diameter of catalyst, D_e is effective diffusion rate, calculated at 0.02 D_v[56]. When the ratio less than 1, the mass transfer limitation within the particle can be ignored.

Reaction kinetics

The removal of 4-CP by all the catalysts follows pseudo-first-order kinetics[57]:

$$\frac{dC}{dt} = -k_{obs} C \quad (5)$$

in the equation, C represents the concentration of 4-CP (mmol L^{-1}), and k_{obs} (min^{-1}) is the fitted pseudo-first-order reaction rate constant. k_{obs} is obtained from the linear regression of the natural logarithm of the solution phase concentration versus time.

Turnover frequency

The initial turnover frequency value (TOF_0, min^{-1}), which is the number of molecules reduced per minute at each site. as follows[58]:

$$TOF_0 = \frac{k_{obs} C_0 M}{C_{Pd} D} \tag{6}$$

where k_{obs} is reaction rate constant, C_0 is initial 4-CP concentration (mol L^{-1}), M is Pd atomic weight (106.4 g mol^{-1}), C_{Pd} is Pd loading (g L^{-1}). TEM analysis shows that Pd NPs are close to spherical, therefore the shape of the NPs is similar to a cubic octahedron[59]. The dispersion of cuboctahedrons is calculated by[59]:

$$D = \frac{30v^2 + 6}{10v^3 + 15v^2 + 11v + 3} \tag{7}$$

where v is the average order of cuboctahedral nanoparticles and calculated[60] by:

$$v = \frac{d}{2d_p} - \frac{1}{2} \tag{8}$$

where d is the nanoparticle diameter obtained from TEM analysis, and d_p is the distance between metal atoms which is equal to 0.275 nm for Pd.

Results and discussion

Characterization

The preparation of nitrogen-doped carbon carrier PMF is based on the co-condensation reaction of mixed resins. As shown in Fig. 1a, a schematic diagram of the preparation of PMF-800 carrier. By mixing phenol, melamine, and formaldehyde, adjusting the pH to 8 with sodium hydroxide, a co-condensation reaction is carried out under a water bath condition at 90 ℃. Phenol and formaldehyde react at a molar ratio of 1:1 to generate phenolic resin, and melamine and formaldehyde react at a molar ratio of 1:1.5 to generate melamine formaldehyde resin, and physical crosslinking occurs between the two resins generated in the subsequent gel and aging process. In this system, melamine serves as a nitrogen source, while phenol and formaldehyde serve as carbon sources. The

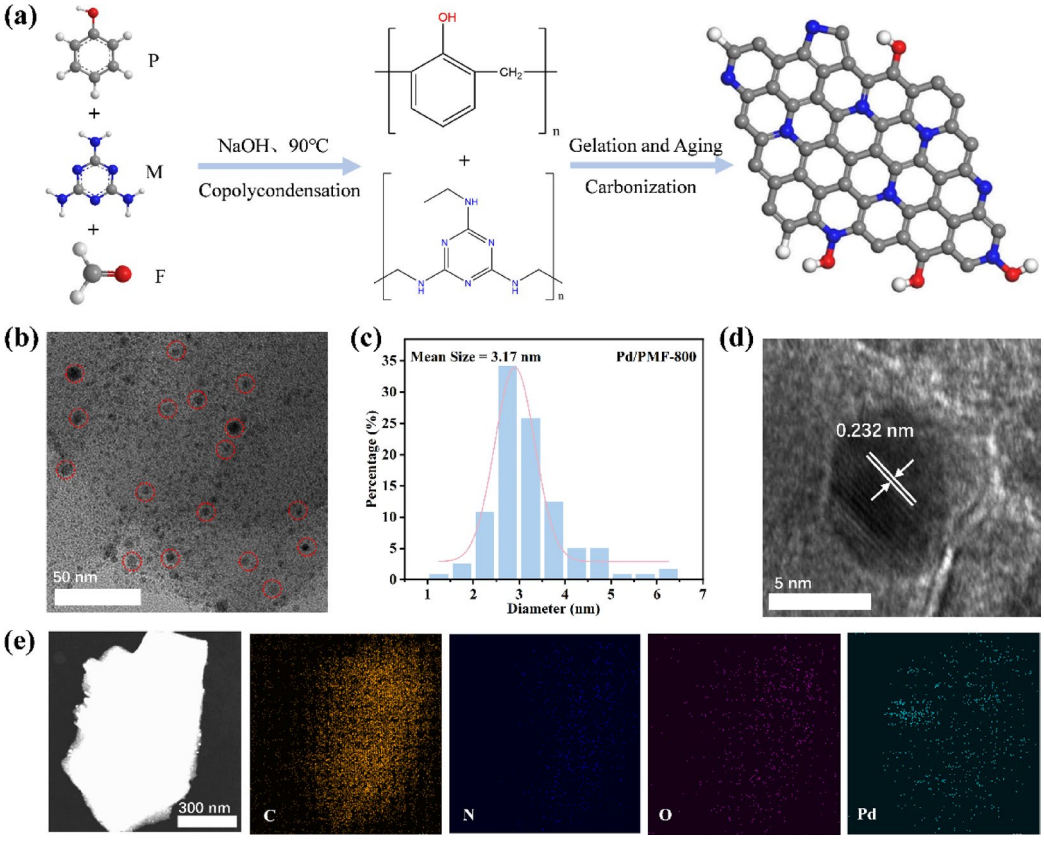

Fig. 1. (**a**) Schematic diagram of PMF-800 carrier preparation process, (**b**) TEM images of Pd/PMF-800 and (**c**)corresponding particle size distribution images, (**d**) HRTEM images of Pd/PMF-800, (**e**) HAADF-STEM images of Pd/PMF-800 and the corresponding elemental mapping images of C, N, O, and Pd.

mixed resin undergoes a series of complex cracking, condensation, and rearrangement during the pyrolysis process, which in turn affects the structure of nitrogen-doped carbon carriers. After heat treatment at 600 ℃, phenolic hydroxyl groups tend to be stabilized, so different carbonization temperatures mainly affect the type of nitrogen in N-doped carbon carriers.

The properties, especially the particle size, of Pd NPs play a crucial role in determining their catalytic activity. To demonstrate the effect of N-doping on the dispersion and size of Pd NPs, the Pd-based catalysts were characterized by TEM, as shown in Fig. 1b and Fig. S1a, d, g. The Pd NPs (marked by a red circle in Fig. 1b) in Pd/PMF are spherical and uniformly dispersed on the surface of the carrier, showing excellent dispersibility. The average particle sizes of Pd NPs on catalysts Pd/AC, Pd/PMF-700, Pd/PMF-800, and Pd/PMF-900 were calculated to be 9.25, 3.45, 3.17, and 3.72 nm, respectively (Fig. 1c and Fig. S1b, e, h), indicating that N-doped has a significant impact on the size of Pd NPs. The high-resolution TEM images (Fig. 1d and Fig. S1c, f, i) reveal the lattice properties of Pd particles. The lattice spacing of approximately 0.23 nm corresponds to the face centered cubic Pd (111) plane. Furthermore, the HAADF-STEM image of representative Pd/PMF-800 and its corresponding elemental mapping images (Fig. 1e) also confirm the homogeneous dispersion of C, N, O and Pd elements.

The XRD pattern of the catalyst is shown in Fig. 2a. Wide diffraction peaks are displayed near $2\theta = 24°$, indicating the successful carbonization of nitrogen-modified phenolic resin. The XRD pattern of Pd NPs is almost consistent with Pd0, and the diffraction peaks at 40.1°, 46.4°, and 68.1° belong to the Pd (111), Pd (200), and Pd (220) phases, respectively. This indicates that Pd NPs have been successfully loaded onto the surface of the carrier and exist in a typical face-centered cubic structure.

In order to further investigate the effect of N-doped on the structure of carbon materials, Raman spectroscopy analysis was performed on three resin carbon catalysts (Fig. 2b). The peak located at 1336 cm^{-1} corresponds to the D band, which is caused by defects in the carbon material. The peak located at 1576 cm^{-1} corresponds to the G band, which is caused by the vibration of sp^2 hybridized carbon atoms in the carbon material. The relative strength ratio (I_D/I_G) between the D and G band is commonly used to represent the degree of graphitization[61]. A higher ratio indicates a lower degree of graphitization. The I_D/I_G ratios of Pd/PMF-700, Pd/PMF-800, and Pd/PMF-900 were found to be 1.06, 1.18, and 1.03, respectively. The I_D/I_G ratio of Pd/PMF-800 is higher than those the other two catalysts, indicating that it has more structural disorder and defect degree, which is more beneficial for improving catalytic performance.

The N-doped degree, chemical bonding of the modified resin carbon carrier and the valence state of the loaded Pd were investigated using XPS. Based on the XPS spectrum in Fig. 3a and the chemical composition in Table 1, the carrier primarily consists of C (~ 285 eV, 81.82 ~ 84.48%), N (~ 402 eV, 5.66 ~ 8.37%), and O (~ 531 eV, 9.81 ~ 10.99%). The XPS measurement spectrum of the catalyst shows a Pd peak, indicating the successful indicating the successful loading of Pd (Fig. 3a). The high-resolution C 1s spectrum can be deconvoluted into three peaks, corresponding to different chemical groups, including C-C/C = C groups (284.8 eV), C-O/C-N groups (285.8 eV), and C = O groups (288.7 eV) (Fig. 3b). Figure 3c illustrates the N 1s spectrum, which was fitted using deconvolution analysis to obtain four peaks corresponding to Pyridine-N (398.1 eV), Pyrrole-N (399.1 eV), Graphite-N (400.8 eV) and Oxidized-N (403.2 eV). The content of each N species in the three resin carbon carriers is listed in Table 2. The difference in electronegativity between heteroatoms and carriers, as well as the higher binding energy between N-doped carriers and metal NPs compared to undoped carriers, enhances the nucleation, catalytic activity, and stability of Pd NPs[62-65]. Among the four different N species, the Pyridine-N species has unhybrid lone pair electrons and strong electron donating ability, which is more conducive to the stability of Pd NPs on the carrier surface. Among the three N-doped catalysts, Pd/PMF-800 has a higher content of Pyridine-N. In the Pd 3d high resolution spectrum (Fig. 3d), the peaks at 335.5 eV and 340.8 eV correspond to Pd^0 in the $3d_{5/2}$ and $3d_{3/2}$ states, while the peaks at 336.7 eV and 341.9 eV correspond to Pd^{2+} in the $3d_{5/2}$ and $3d_{3/2}$ states, respectively. This indicates that Pd in the catalyst exists in both Pd^0 and Pd^{2+}states. Fig. S2 is the spectrum of Pd 3d after five cycles of reaction. The content of Pd in different valence states is presented in Table S2. Figure 3e is a schematic diagram of the N-binding types in the phenolic resin carbon support. The ratios of

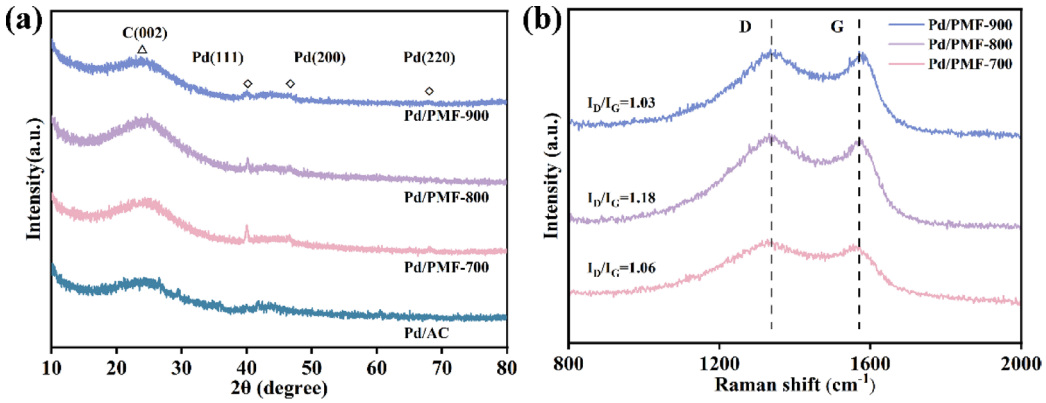

Fig. 2. (**a**) XRD pattern of Pd based modified resin carbon and activated carbon catalyst, (**b**) Raman spectra of palladium based modified resin carbon catalyst.

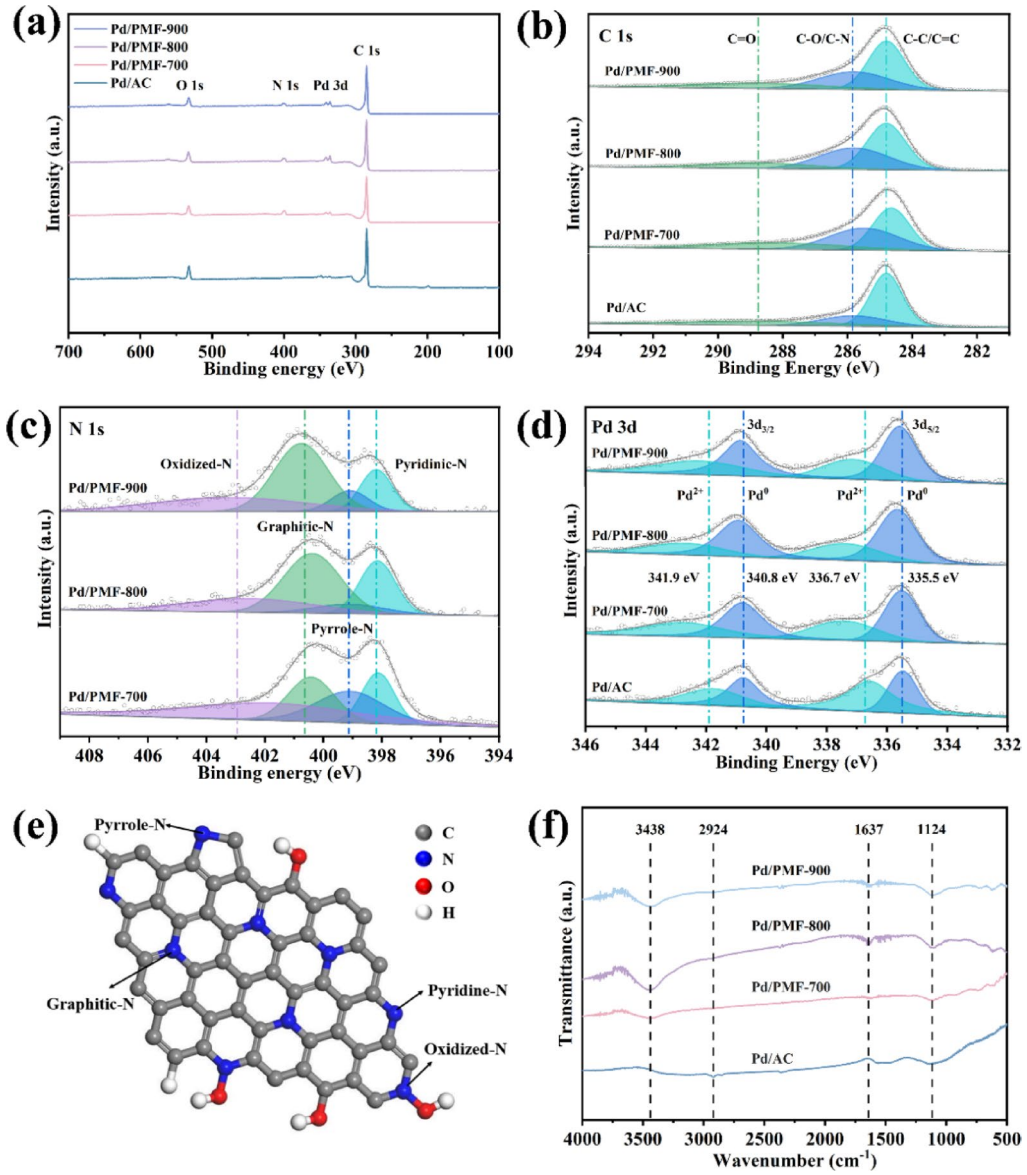

Fig. 3. (**a**) XPS spectra of all samples, high-resolution XPS spectra of (**b**) C 1s, (**c**) N 1s and (**d**) Pd 3d, (**e**) Schematic diagram of N binding types in carbon structure, (**f**) FTIR spectrogram of modified polymer resin.

Carrier	Content (%)			Proportion of various nitrogen species			
	C	O	*N*	Pyridine nitrogen	Pyrrole nitrogen	Graphite nitrogen	Nitrogen oxide
PMF-700	81.82	9.81	8.37	20.0	26.2	25.1	28.7
PMF-800	82.11	10.99	6.90	24.8	8.7	44.3	22.2
PMF-900	84.48	9.86	5.66	17.5	10.0	47.8	24.7

Table 2. XPS analysis of the content of modified resin carriers C, N, O, and the proportions of various nitrogen species.

$Pd^0/(Pd^0 + Pd^{2+})$ in fresh catalysts Pd/AC, Pd/PMF-700, Pd/PMF-800, and Pd/PMF-900 are 46.8%, 59.5%, 65.4%, and 57.9%, respectively. The catalytic hydrodechlorination reaction requires Pd^0 and Pd^{2+}. The Pd sites have dual properties and are composed of the combination of two substances: electron-deficient Pd^{2+} and metallic Pd^0[66].

From the FTIR spectrum shown in Fig. 3f, it is evident that the samples obtained at different carbonization temperatures exhibit similar spectra, indicating that changes in carbonization temperature will not affect the chemical structure of N-doped resin carbon carriers. The strong and broad absorption peak at 3438 cm^{-1} corresponds to the O-H stretching vibration of hydroxyl groups and the stretching vibration of N-H bonds. The

Catalyst	$a \times k_c$ (s^{-1})	k_{obs} (s^{-1})	$k_{obs} \times D_c^2/D_e$
Pd/AC	3.2×10^{-2}	7.6×10^{-5}	4.8×10^{-2}
Pd/PMF-700	1.6×10^{-2}	4.8×10^{-4}	3.1×10^{-1}
Pd/PMF-800	1.5×10^{-2}	9.9×10^{-4}	6.3×10^{-1}
Pd/PMF-900	1.6×10^{-2}	6.9×10^{-4}	4.4×10^{-1}

Table 3. Mass transfer rate constant ($a \times k_c$), reaction rate constant (k_{obs}), and Weisz and Prater criteria ($k_{obs}D_c^2/D_e$) for liquid-solid mass transfer within particles at pH = 7.

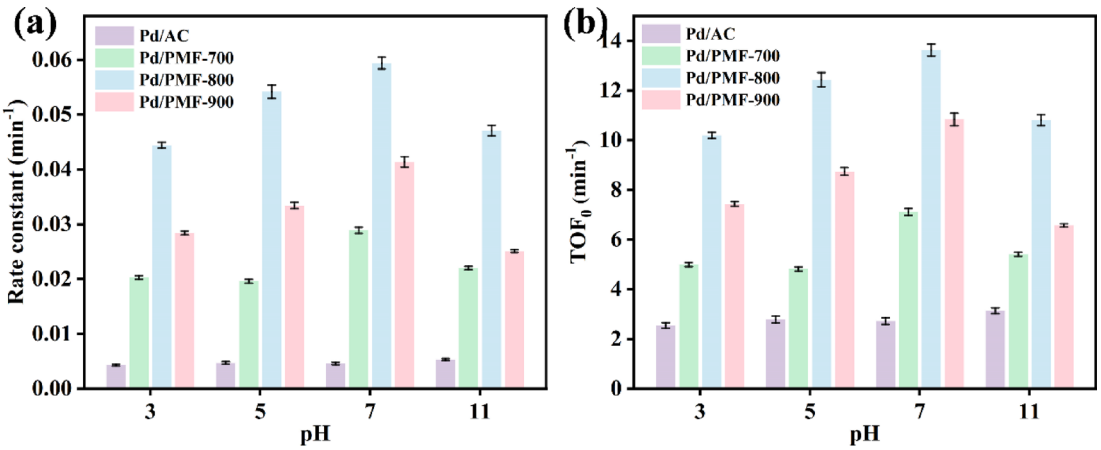

Fig. 4. (**a**) The rate constant of 4-CP reduction, (**b**) the initial turnover frequency. The pH values of the catalyst are 3, 5, 7, 11, 4-CP (12 mg), solvent (1 mL), catalyst 10 mg.

peak at 2924 cm^{-1} is attributed to the stretching vibration of C-H bonds. The peak at 1637 cm^{-1} corresponds to the tensile vibration of C-N bonds, further confirming the presence of N-doped in the skeleton structure of the modified resin, which is consistent with the conclusion of XPS. The peak at 1124 cm^{-1} corresponds to the C-O stretching vibration of aromatic ether. It should be noted that when a substance is subjected to different carbonization temperatures, the infrared spectral positions of its constituents may shift[67]. This phenomenon occurs because the groups present in the substance undergo decomposition of or transformation into other functional groups at high temperatures, leading to changes in the structure and chemical composition of the material, resulting in shifts in the absorption peak positions in the infrared spectrum.

Mass transfer

The catalytic activity of the reaction system is influenced by the mass transfer rate both outside and inside the catalyst particles[68]. Smaller particle sizes and higher mixing rates contribute to reducing the impact of mass transfe limitations[31]. The calculated external mass transfer rate constant is greater than the measured observed rate constant (k_{obs}) (Table 3). Therefore, the influence of solid-liquid mass transfer on the reaction can be ignored, since an explanation for ignoring the influence of mass transfer limitations outside the particles is that the catalyst particles are smaller ($< 1.8 \times 10^{-1}$ mm). Therefore, the external mass transfer limitations in the development and evaluation of the modified resin carbon catalyst can be ignored. As shown in Table 2, the calculated values of the Weisz and Prater criteria for both the modified resin carbon catalysts and activated carbon catalysts are less than 1. This indicates that the reduction rate of 4-CP on the surface of Pd NPs is significantly slower than its diffusion rate through the internal pores. As a result, the mass transfer limitations within the particles can also be disregarded.

Effect of pH

The change in pH value of the solution can have an impact on the catalytic activity of the catalyst to a certain extent[69]. Wastewater containing 4-CP is generated in industrial processes, and the pH value varies depending on the production process. Therefore, it is crucial to develop a catalyst that can rapidly and efficiently degrade 4-CP in industrial wastewater with different pH values. As shown in Fig. 4a, the reduction rate constants (k_{obs}) of the four catalysts were determined at pH 3, 5, 7 and 11 in 4-CP solution. The k_{obs} of the three modified resin carbon catalysts, Pd/PMF-700, Pd/PMF-800, and Pd/PMF-900, exhibited an increasing trend from pH 3 to 11, followed by a decrease. At pH 7, they reached their highest k_{obs}, which were 0.0289, 0.0594, and 0.0414 min^{-1} (Table S1). Pd/PMF-800 exhibited higher k_{obs} than other catalysts at different pH conditions. The TOF_0 also exhibits the same trend (Fig. 4b). The dechlorination rate of Pd/AC is less affected by pH changes, with dechlorination rates ranging from 19.06 to 22.7%, which is lower than the activity of resin carbon catalysts.

As shown in Fig. 5, the HDC kinetics of 4-CP under different pH values were studied using Pd/PMF-800 as the catalyst. At pH 3, 5, 7, and 11, the required time for complete dechlorination of 4-CP is 80, 70, 60, and 80 min, respectively. In acidic solutions, the presence of high concentrations of Cl^- forms $PdCl_3^-$ and $PdCl_4^{2-}$ with Pd NPs on the surface of resin-carbon carriers. Compared with the Pd^0 and Pd^{2+}species required for 4-CP HDC, $PdCl_3^-$ and $PdCl_4^{2-}$ have no activity in the dechlorination of 4-CP[70]. The formation of $PdCl_3^-$ and $PdCl_4^{2-}$ also leads to the leaching of Pd NPs from the surface of the resin carbon support during the reaction process, reducing the activity of the catalyst. In alkaline solution, the precipitation of metal hydroxides formed on the surface of resin-carbon support leads to passivation of the catalyst surface. Therefore, the activity of the catalyst decreases in alkaline solutions, leading to a decrease in the dechlorination effeciency of 4-CP[71,72]. Although the complete dechlorination time of 4-CP is extended in both acidic and alkaline solutions, it can still be achieved within a relatively short time, indicating the ability of Pd/PMF-800 in adapting to various pH values and exhibit strong acid-base stability and adaptability. Catalysts can maintain their catalytic activity under different acid-base conditions, which is of great significance for many catalytic reactions.

Effect of reaction temperature

A series of experiments were conducted at 30–75 ℃ to investigate the effect of resin carbon catalysts on 4-CP HDC at different temperatures. The dechlorination rate of 4-CP is shown in Fig. S4. Temperature changes have a certain impact on 4-CP HDC[73]. Taking the Pd/PMF-800 catalyst as an example, within 60 min, the removal rate of 4-CP was only 46.2% at 30 ℃, 72.54% at 45 ℃, and 100% at 60 ℃. When the temperature rises to 75 ℃, 4-CP achieves complete removal within 30 min. The pseudo first-order reaction kinetics were used to compare the catalytic performance of the four resin carbon catalysts at different temperatures. As shown in Fig. S5 and Table S1, at reaction temperatures of 30, 45, 60, and 75 ℃, the reaction rate constants for the removal of 4-CP by Pd/PMF-800 are 0.0102, 0.0225, 0.0594, and 0.1291 min^{-1}. The dechlorination activity increased with increasing temperature[73]. Further fitting the activation energy of the reaction using the Arrhenius equation (Fig. 6). The activation energies of 4-CP HDC under the four catalyst conditions of Pd/AC, Pd/PMF-700, Pd/PMF-800, and Pd/PMF-900 are 60.3 kJ mol^{-1}, 53.1 kJ mol^{-1}, 47.1 kJ mol^{-1}, and 51.4 kJ mol^{-1}, respectively, which are lower than the C-Cl bond dissociation energy (341.0 kJ mol^{-1})[74]. The experimental results indicate that N modified resin catalysts exhibit high catalytic activity and can significantly reduce the activation energy of dechlorination reactions. When using Pd/PMF-800 catalyst, the activation energy required for 4-CP HDC is the lowest.

Extensive research

In order to investigate the widespread applicability of Pd/PMF-800 catalyst, hydrodehalogenation experiments were conducted on 2-CP and 4-BP. Figure 7 shows the experimental results of hydrodehalogenation for these two different halogenated phenols. The TOF_0 of the halogenated phenols follows the order of 4-BP > 4-CP > 2-CP (TOF_0 values are 15.3, 13.6, and 5.6 min^{-1}, respectively). The binding energy of 4-BP is 280 kJ mol^{-1} and the binding energy of 2-CP and 4-CP are 341 kJ mol^{-1}. 4-BP can dehalogenate in a shorter time due to its lower binding energy. The dechlorination rate of 2-CP within 60 min is 90.02%, and 4-BP can completely dehalogenate within 40 min. The reaction rate constants for the removal of 2-CP and 4-BP by Pd/PMF-800 catalyst are 0.0246 min^{-1} and 0.0666 min^{-1}, respectively. The conversion frequency for 2-CP and 4-CP are consistent with the results reported by Xia et al.[75]. They found that in the hydrogenation reaction of monochlorophenol in aqueous solution, the hydroxyl ortho C-Cl bond is the most difficult to dechlorinate compared to the meta and para C-Cl bonds. The steric hindrance effect of hydroxyl groups has a certain impact on the hydrogenolysis of ortho C-Cl bonds.

Catalyst longevity

Test the reactivity of the catalyst in five consecutive cyclic reactions to investigate its stability (Fig. 8). After five cycles of reaction, the activity of the Pd/AC catalyst decreased to 1.01%. After the same number of cycles, the activities of Pd/PMF-700, Pd/PMF-800, and Pd/PMF-900 decreased to 71.31%, 91.56% and 69.82%, respectively.

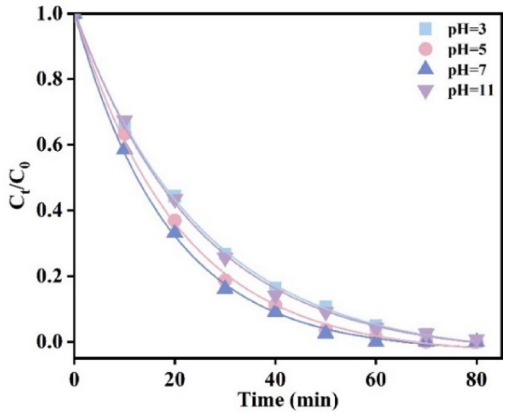

Fig. 5. HDC kinetics of 4-CP under different pH values under Pd/PMF-800 conditions. Conditions: 4-CP (12 mg), solvent (1 mL), catalyst 10 mg, 0.1 MPa H_2, 60 ℃, 80 min.

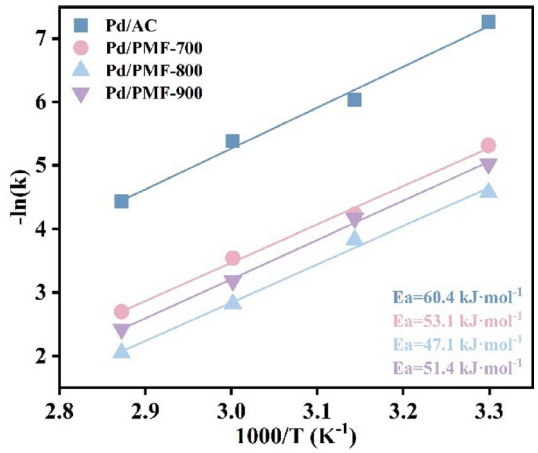

Fig. 6. Fitting the relationship between reaction rate constant and temperature using Arrhenius equation.

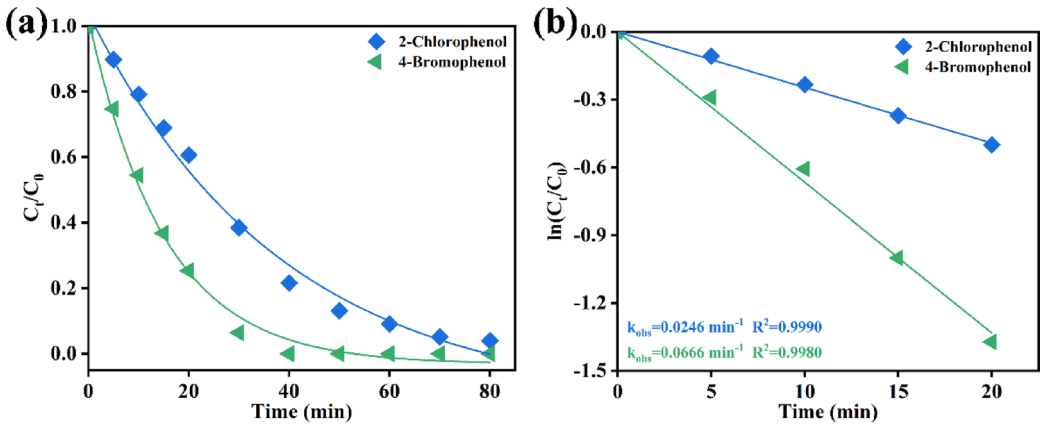

Fig. 7. (**a**) The hydrogenation and dehalogenation kinetics of Pd/PMF-800 catalysts on 2-CP and 4-BP, respectively. (**b**) Plots of $\ln(C_t/C_0)$ versus reaction time over Pd/PMF-800. Reaction conditions: The molar ratio of substrate to Pd content is the same, 2-CP (12 mg), 4-BP (16 mg), deionized water (1 mL), pH = 7, catalyst 10 mg, 0.1 MPa H_2, 60 ℃, 80 min.

Notably, after five consecutive cycles of reaction, the Pd/PMF-800 resin catalyst did not show significant Pd loss (Table S3). The excellent stability of 4-CP HDC depends on the strong interaction between Pd NPs and the carrier, which limits the loss of Pd NPs on the catalyst surface. As the number of cycles increased, the degradation rate of 4-CP for all four catalysts showed a decreasing trend, suggesting that the catalyst surface may undergo some changes after repeated use.

The catalyst was recovered after five cycles of experiments and characterized using TEM and XPS. The TEM image of Pd/PMF-800 is shown in Fig. S6a, revealing no significant aggregation of Pd NPs. The particle size distribution diagram is shown in Fig. S6b, confirming the slight growth of Pd NPs between 3.17 and 3.54 nm. This partial increase in size is one of the reasons for the decreased activity of Pd/PMF-800 after five cycles. Additionally, by comparing the Pd 3d XPS spectra of Pd/PMF-800 before and after the cyclic experiment (Fig. S6d), it was observed that the ratio of $Pd^0/(Pd^0 + Pd^{2+})$ decreased from 65.4 to 54.8%. This indicates a significant change in the valence state of Pd^0 during the repeated dechlorination experiment. By combining XPS and TEM results, we can conclude that there are slight changes between fresh and used catalysts, the size of Pd NPs and the ratio of $Pd^0/(Pd^0 + Pd^{2+})$ have a significant impact on the catalytic performance in HDC reactions.

Conclusions

In this work, N-doping phenolic resin carbon catalysts were successfully synthesized based on the co-polycondensation reaction of mixed resins, with phenol and formaldehyde as the C source and melamine as the N source. Specifically, the N-doped causes structural distortion, changes in charge density, and electronic structure modulation in resin carbon materials, promoting electronegativity differences between N and resin carbon carriers, and improving the nucleation, stability, and dispersion of Pd NPs on the surface of resin carbon carriers. The required activation energy for 4-CP HDC under the conditions of Pd/PMF-800 catalyst is 47.1 kJ mol^{-1}. Among them, Pd/PMF-800 showed excellent activity and stability towards 4-CP HDC. At a pH of 7 and

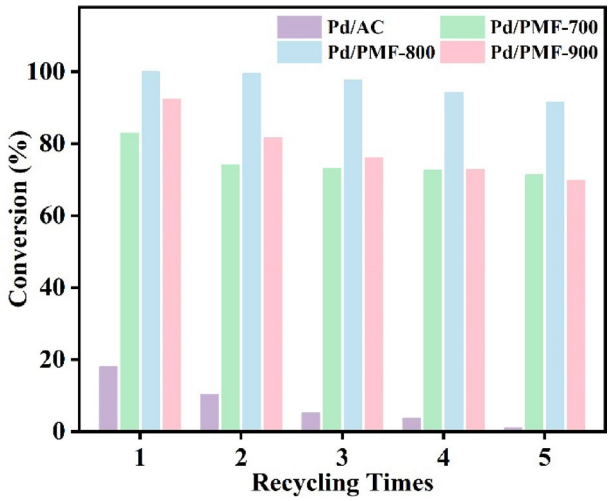

Fig. 8. The reusability of Pd/AC, Pd/PMF-700, Pd/PMF-800, and Pd/PMF-900 catalysts for 4-CP HDC. Conditions: 4-CP (12 mg), deionized water (1 mL), pH = 7, catalyst 10 mg, 0.1 MPa H_2 pressure, 60 ℃, 60 min.

a reaction temperature of 60 ℃, it achieved complete degradation of 4-CP within 60 min, after 5 cycles of testing the dechlorination rate was 91.56%. Pd/PMF-800 has a higher Pyridine-N (24.8%) and a higher $Pd^0/(Pd^{2+}+Pd^0)$ ratio (65.4%), which is more beneficial for improving catalytic performance. Importantly, the catalyst has broad applicability and exhibits high activity towards various halogenated phenols. It achieves a dechlorination rate of 90.02% for 2-CP in 60 min and complete debromination for 4-BP in 40 min. At the same time, the catalyst also has the characteristic of a wide range of pH values. We hope that this work can provide a catalyst with efficient dehalogenation, strong acid-base stability and adaptability, and recyclability for the degradation of halogenated phenols in the environment.

Data availability

All data generated or analysed during this study are included in this published article [and its supplementary information files].

Received: 3 January 2025; Accepted: 6 June 2025
Published online: 01 July 2025

References

1. Long, M. et al. *Para-Chlorophenol (4-CP) Removal by a Palladium-Coated Biofilm: Coupling Catalytic Dechlorination and Microbial Mineralization Via Denitrification* 556309–6319 (Environmental Science & Technology, 2021).
2. Xiong, J., Ma, Y., Yang, W. & Zhong, L. Rapid, highly efficient and stable catalytic hydrodechlorination of Chlorophenols over novel Pd/CNTs-Ni foam composite catalyst in continuous-flow. *J. Hazard. Mater.* **355**, 89–95 (2018).
3. Hu, T., Liu, T., Xu, C., Liu, M. & Zhou, S. Simultaneous construction of silica nanotubes loaded with Pd nanoparticles for catalytic hydrodechlorination of Chlorophenols. *ACS Appl. Nano Mater.* **4**, 10692–10700 (2021).
4. Xiao, M. et al. Recyclable heterogeneous Pd nanoparticles supported on plant polyphenol-modified γ-Al_2O_3 for hydrodechlorination of 2,4-dichlorophenols. *Bull. Mater. Sci.* **43**, 215 (2020).
5. Mao, J. et al. Biochar-supported atomically dispersed copper as cost-effective and adaptable catalysts for heterogeneous activation of peroxymonosulfate towards the degradation of Chlorophenol. *J. Environ. Chem. Eng.* **12**, 114500 (2024).
6. Meng, J. et al. The coordination bond reinforced FeOCl/C_3N_4 heterostructure for photocatalytic degradation of persistent organic pollutants. *J. Environ. Chem. Eng.* **12**, 114404 (2024).
7. Ruiz-Garcia, C. et al. Improving the activity in hydrodechlorination of pd/c catalysts by nitrogen doping of activated carbon supports. *J. Environ. Chem. Eng.* **8**, 103689 (2020).
8. Alexandre, J. C., Rodrigues, P. R. M. & de Lucena, S. M. P. Prediction of Chlorophenols adsorption on activated carbons by representative pores method. *Environ. Sci. Pollut. Res.* **29**, 79866–79874 (2022).
9. Zhang, X. et al. Development of highly efficient and reusable magnetic nitrogen-doped carbon nanotubes for Chlorophenol removal. *Environ. Sci. Pollut. Res.* **28**, 37424–37434 (2021).
10. Zhong, J., Li, W., Xie, Y., Yang, Y. & Ding, L. Interaction between Chlorophenols in the adsorption process on corn straw Biochar. *Desalination Water Treat.* **290**, 104–112 (2023).
11. Kwean, O. S. et al. 4-Chlorophenol biodegradation facilitator composed of Recombinant multi-biocatalysts immobilized onto montmorillonite. *Bioresour. Technol.* **259**, 268–275 (2018).
12. Zhou, Z., Yuan, W., Wu, Y., Fu, H. & Wang, Z. Toxicity, degradation and metabolic pathway of 4-chlorinephenol in Chlorella vulgaris. *Desalination Water Treat.* **320**, 100729 (2024).
13. Sun, S. et al. Bioremediation mechanisms of chlorophenol-Cr(1V): the role of amines, immobilization, and DEGs in Pseudomonas sp. PC. *Chem. Eng. J.* **497**, 154318 (2024).
14. Hao, Q. et al. Bi_2O_3@Carbon nanocomposites for Solar-Driven photocatalytic degradation of Chlorophenols. *ACS Appl. Nano Mater.* **2**, 2308–2316 (2019).
15. Kotlhao, K. et al. Enhancing the photocatalytic degradation of selected Chlorophenols using ag/zno nanocomposites. *MRS Adv.* **3**, 2129–2136 (2018).
16. Wang, Y. et al. Fabrication of core-shell shaped heterojunction Bi2MoO6/ln2O3 nanofibers as a highly efficient photocatalyst toward degradation of 4-chlorophenol. *J. Water Process. Eng.* **69**, 106702 (2025).

17. Liu, L., Hao, S., Liu, J., Zhou, H. & Hu, X. Removal of phenol from wastewater by electrochemical bromination in a flow reactor. *Environ. Sci. Pollut. Res.* **29**, 88681–88689 (2022).
18. Zhang, J. et al. Electrochemical-driven nanoparticulate catalysis for highly efficient dechlorination of chlorinated environmental pollutant. *J. Catal.* **395**, 362–374 (2021).
19. Yang, K., Abu-Reesh, I. M. & He, Z. Degradation of 4-chlorophenol through cooperative reductive and oxidative processes in an electrochemical system. *J. Hazard. Mater.* **442**, 130126 (2023).
20. Chen, X. et al. Interfacial microenvironment effects on electrochemical CO2 reduction. *Chem. Eng. J.* **482**, 148944 (2024).
21. Zhang, W., Wang, F., Li, X., Liu, Y. & Ma, J. Pd nanoparticles modified rod-like nitrogen-doped ordered mesoporous carbons for effective catalytic hydrodechlorination of Chlorophenols. *RSC Adv.* **6**, 27313–27319 (2016).
22. Zhan, Y. et al. Catalytic dechlorination and deep hydrogenation of 4-chlorophenol in a hydrogen-based internal circulation reactor for efficient wastewater detoxification. *J. Water Process. Eng.* **60**, 105148 (2024).
23. Li, Z. et al. Enhanced catalytic performance induced by synergistic interaction between Pd species with NiAl2O4 spinel support for aqueous-phase hydrodechlorination of 4-chlorophenols. *Chem. Eng. J.* **497**, 154399 (2024).
24. Qiao, J., Zhao, Z., Zhou, Z. & Wu, D. Enhanced hydrodechlorination of 4-chlorophenol through carboxymethylcellulose-modified pd/fe nanosuspension synthesized by one-step methods. *Chemosphere* **356**, 141857 (2024).
25. Xu, J., Zhang, S., Liu, X., Bian, F. & Jiang, H. Rh/polymeric carbon nitride porous tubular catalyst: visible light enhanced Chlorophenol hydrodechlorination in base-free aqueous medium. *Catal. Sci. Technol.* **9**, 6938–6945 (2019).
26. Mahy, J. G., Tasseroul, L., Tromme, O., Lavigne, B. & Lambert, S. D. Hydrodechlorination and complete degradation of chlorinated compounds with the coupled action of Pd/SiO_2 and Fe/SiO_2 catalysts: towards industrial catalyst synthesis conditions. *J. Environ. Chem. Eng.* **7**, 103014 (2019).
27. Xiong, J., Tian, L. & Cheng, R. Promoted catalytic hydrodechlorination for deep degradation of Chlorophenols over $Rh\text{-}La/SiO_2$ catalyst. *J. Hazard. Mater.* **416**, 125913 (2021).
28. Lee, S. R. et al. Selective hydrodechlorination of trichloromethane to dichloromethane over bimetallic Pt-Pd/KIT-6: catalytic activity and reaction kinetics. *Chem. Eng. J.* **331**, 556–569 (2018).
29. Xie, Q., Lei, C., Chen, W. & Huang, B. Mesoporous ferrihydrite-supported Pd nanoparticles for enhanced catalytic dehalogenation of chlorinated environmental pollutant. *J. Colloid Interface Sci.* **608**, 2907–2920 (2022).
30. Tian, L. et al. High performance of metal modified Pd catalyst for hydrodechlorination of Chlorophenols to cyclohexanone. *Reaction Kinetics Mech. Catal.* **135**, 741–753 (2022).
31. Jadbabaei, N., Ye, T., Shuai, D. & Zhang, H. Development of palladium-resin composites for catalytic hydrodechlorination of 4-chlorophenol. *Appl. Catal. B.* **205**, 576–586 (2017).
32. Zhou, G. et al. *Efficient Activation of Peroxymonosulfate by Cobalt Supported Used Resin* (Based Carbon Ball Catalyst for the Degradation of Ibuprofen, 2022).
33. Zhao, J. et al. Highly efficient synthesis of dimethyl carbonate over copper catalysts supported on resin-derived carbon microspheres. *Chem. Eng. Sci.* **207**, 1060–1071 (2019).
34. Munoz, M. et al. Polymer-based spherical activated carbon as catalytic support for hydrodechlorination reactions. *Appl. Catal. B.* **218**, 498–505 (2017).
35. Zhang, T. & Asefa, T. Heteroatom-Doped carbon materials for hydrazine oxidation. *Adv. Mater.* **31**, 1804394 (2019).
36. Chen, Z. & Li, H. The lithium ions storage behavior of heteroatom-mediated echinus-like porous carbon spheres: from co-doping to multi-atom doping. *J. Colloid Interface Sci.* **567**, 54–64 (2020).
37. Bisen, O. Y., Nandan, R. & Nanda, K. K. Unique One-Step strategy for nonmetallic and metallic heteroatom doped carbonaceous materials. *ACS Omega*. **5**, 32852–32860 (2020).
38. Wang, Z. et al. Synergistic effects of phosphorus/nitrogen co-doping and morphology regulation enhance the catalytic hydrogenation performance of Ru-based catalysts for benzoic acid. *New J. Chem.* **47**, 14819–14827 (2023).
39. Wang, F. et al. N-doped honeycomb-like porous carbon towards high-performance supercapacitor. *Chin. Chem. Lett.* **31**, 1986–1990 (2020).
40. Li, P. et al. N-doped interconnected porous graphene as advanced electrode material for supercapacitors. *J. Alloys Compd.* **893**, 162218 (2022).
41. Dai, S. et al. A high-performance supercapacitor electrode based on N-doped porous graphene. *J. Power Sources*. **387**, 43–48 (2018).
42. Kong, X., Gai, P., Ge, L. & Li, F. Laser-Scribed N-Doped graphene for integrated flexible enzymatic biofuel cells. *ACS Sustain. Chem. Eng.* **8**, 12437–12442 (2020).
43. Jiang, D. et al. Polyaniline@N-doped macroporous carbon foam as self-supporting anodes for microbial fuel cells. *Int. J. Hydrog. Energy*. **47**, 35458–35467 (2022).
44. Massaglia, G. et al. Nonwoven Mats of N-doped carbon nanofibers as high-performing anodes in microbial fuel cells. *Mater. Today Energy*. **16**, 100385 (2020).
45. Ragu, S., Kim, B., Chen, S. M., Ishfaque, A. & Kang, K. M. N-substituted CQDs impregnated by Fe_3O_4 heterostructure: bifunctional catalyst for electro-catalytic and photo-catalytic detection of an environmental hazardous organic pollutant. *Chemosphere* **311**, 137168 (2023).
46. Novodchuk, I. et al. An ultrasensitive heart-failure BNP biosensor using B/N co-doped graphene oxide gel FET. *Biosens. Bioelectron.* **180**, 113114 (2021).
47. Quintero-Jaime, A. F., Quílez-Bermejo, J., Cazorla-Amorós, D. & Morallón, E. Metal free electrochemical glucose biosensor based on N-doped porous carbon material. *Electrochim. Acta*. **367**, 137434 (2021).
48. Xu, J., Wang, Y. H., Wei, Z., Wang, F. T. & Huang, K. J. Significantly improving the performance of self-powered biosensor by effectively combining with high-energy enzyme biofuel cells, N-doped graphene, and ultrathin Hollow carbon shell. *Sens. Actuators B*. **327**, 128933 (2021).
49. Bilal, S., Sami, A. J., Hayat, A., Fayyaz ur, M. & Rehman Assessment of pesticide induced Inhibition of Apis mellifera (honeybee) acetylcholinesterase by means of N-doped carbon dots/bsa nanocomposite modified electrochemical biosensor. *Bioelectrochemistry* **144**, 107999 (2022).
50. Li, Z. et al. Cost-Effective monolithic hierarchical carbon cryogels with nitrogen doping and High-Performance mechanical properties for CO_2 capture. *ACS Appl. Mater. Interfaces*. **12**, 21748–21760 (2020).
51. Li, X., Zhang, J. & Li, W. MOF-derived nitrogen-doped porous carbon as metal-free catalysts for acetylene hydrochlorination. *J. Ind. Eng. Chem.* **44**, 146–154 (2016).
52. Hu, X. et al. Nitrogen-doped agar-derived porous carbon with long cycle life for high-performance ionic liquid-based supercapacitors. *Diam. Relat. Mater.* **139**, 110332 (2023).
53. Harriott, P. Mass transfer to particles: part I. Suspended in agitated tanks. *AIChE J.* **8**, 93–101 (1962).
54. Saltzman, E. S., King, D. B., Holmen, K. & Leck, C. Experimental determination of the diffusion coefficient of dimethylsulfide in water. *J. Geophys. Research: Oceans*. **98**, 16481–16486 (1993).
55. Bidabehere, C. M., García, J. R. & Sedran, U. Transient effectiveness factors in the dynamic analysis of heterogeneous reactors with porous catalyst particles. *Chem. Eng. Sci.* **137**, 293–300 (2015).
56. Walters, E. A. A new sun the solar results from Skylab (Eddy, John A). *J. Chem. Educ.* **57**, A297 (1980).
57. Sharma, A. et al. Rietveld refinement, morphological, optical and photocatalytic dye degradation studies of pristine and Sr-Doped SnS_2 hexagonal nanoplates. *Mater. Res. Bull.* **168**, 112464 (2023).

58. Shuai, D. et al. Structure sensitivity study of waterborne contaminant hydrogenation using Shape- and Size-Controlled Pd nanoparticles. *ACS Catal.* **3**, 453–463 (2013).
59. Shuai, D., Choe, J. K., Shapley, J. R. & Werth, C. J. *Enhanced Activity and Selectivity of Carbon Nanofiber Supported Pd Catalysts for Nitrite Reduction* 462847–2855 (Environmental Science & Technology, 2012).
60. Wu, C. W., Chiang, M. H. & Lee, C. L. Pd@Au Core-Shell octahedral, truncated octahedral, and cubic nanocrystals as nonenzymatic glucose sensors for drinks. *Microchem. J.* **190**, 108697 (2023).
61. Ikhtiarini, N., Tjahjanto, R. T. & Setianingsih, T. The effect of parameter combinations (Carbonization Temperature - Chemical Activator) on degree of graphitization, aromaticity, and fungsional group of Rose petal (Rosa sp) Based-Activated carbon. *IOP Conf. Series: Mater. Sci. Eng.* **546**, 022007 (2019).
62. Nguyen, V. T. et al. Effects of graphitic and pyridinic nitrogen defects on transition metal nucleation and nanoparticle formation on N-Doped carbon supports: implications for catalysis. *ACS Appl. Nano Mater.* **5**, 14922–14933 (2022).
63. An, N. et al. High-performance palladium catalysts for the hydrogenation toward dibenzylbiotinmethylester: effect of carbon support functionalization. *J. Colloid Interface Sci.* **510**, 181–189 (2018).
64. Li, R. et al. Pd supported on N-doped-ordered mesoporous carbons' catalysts for selective hydrodechlorination of 4-chlorophenol. *Chem. Pap.* **72**, 2425–2432 (2018).
65. Arrigo, R. et al. Nature of the N–Pd interaction in Nitrogen-Doped carbon nanotube catalysts. *ACS Catal.* **5**, 2740–2753 (2015).
66. Gómez-Sainero, L. M., Seoane, X. L., Fierro, J. L. G. & Arcoya, A. Liquid-Phase hydrodechlorination of CCl_4 to $CHCl_3$ on pd/carbon catalysts: nature and role of Pd active species. *J. Catal.* **209**, 279–288 (2002).
67. Li, Y., Xiong, X., Zhang, C. & Liu, A. Sustainable restoration of anoxic freshwater using environmentally-compatible oxygen-carrying biochar: performance and mechanisms. *Water Res.* **214**, 118204 (2022).
68. Zhang, T. et al. Co@C nanorods as both magnetic stirring nanobars and magnetic recyclable nanocatalysts for microcatalytic reactions. *Appl. Catal. B.* **304**, 120925 (2022).
69. Wang, Q. et al. Selective degradation of Parachlorophenol using Fe/Fe3O4@CPPy nanocomposites via the dual nonradical/radical peroxymonosulfate activation mechanisms. *Chem. Eng. J.* **445**, 136806 (2022).
70. Diaz, E. et al. Comparison of activated carbon-supported Pd and Rh catalysts for aqueous-phase hydrodechlorination. *Appl. Catal. B.* **106**, 469–475 (2011).
71. Jeon, J., Park, Y. & Hwang, Y. Catalytic hydrodechlorination of 4-Chlorophenol by Palladium-Based catalyst supported on alumina and graphene materials. *Nanomaterials* **13**, 1564 (2023).
72. RautS.S., Shetty, R., Raju, N. M., Kamble, S. P. & Kulkarni, P. S. Screening of zero valent mono/bimetallic catalysts and recommendation of Raney Ni (without reducing agent) for dechlorination of 4-chlorophenol. *Chemosphere* **250**, 126298 (2020).
73. Chang, W., Kim, H., Oh, J. & Ahn, B. J. Hydrodechlorination of Chlorophenols over Pd catalysts supported on zeolite Y, MCM-41 and graphene. *Res. Chem. Intermed.* **44**, 3835–3847 (2018).
74. Long, X. et al. Ultrafine Pd nanoparticles@g-C_3N_4 for highly efficient dehalogenation of chlorinated environmental pollutant: structure, efficacy and mechanisms. *Sci. Total Environ.* **775**, 145178 (2021).
75. Chen, N., Rioux, R. M. & Ribeiro, F. H. Investigation of reaction steps for the hydrodechlorination of Chlorine-Containing organic compounds on Pd catalysts. *J. Catal.* **211**, 192–197 (2002).

Acknowledgements

The Key R&D Project of Zhejiang Province (No. 2021C03163).

Author contributions

Zhengyu Pan: Writing-Original draft preparation, Formal analysis. Xianlang Chen：Formal analysis. Zijian Wang: Validation. Rongrong Li: Conceptualization, Methodology. Tongyang Song: Conceptualization, Methodology. Yuhao Cai: Validation. Deman Han: Conceptualization, Writing-Reviewing and Editing. Jianrong Chen: Conceptualization, Supervision, Writing-Reviewing and Editing, Project administration, Funding acquisition.

Declarations

Competing interests

The authors declare no competing interests.

Additional information

Supplementary Information The online version contains supplementary material available at https://doi.org/10.1038/s41598-025-06159-7.

Correspondence and requests for materials should be addressed to D.H. or J.C.